

Valley-dependent transport in strain engineering graphene heterojunctions

Fei Wan(万飞), X R Wang(王新茹), L H Liao(廖烈鸿), J Y Zhang(张嘉颜),M N Chen(陈梦南), G H Zhou(周光辉), Z B Siu(萧卓彬), Mansoor B. A. Jalil, and Yuan Li(李源)

Citation: Chin. Phys. B, 2022, 31 (**7**): 077302. DOI: 10.1088/1674-1056/ac5613
Journal homepage: http://cpb.iphy.ac.cn; http://iopscience.iop.org/cpb

What follows is a list of articles you may be interested in

Half-metallicity induced by out-of-plane electric field on phosphorene nanoribbons

Xiao-Fang Ouyang(欧阳小芳) and Lu Wang(王路)
Chin. Phys. B, 2022, 31 (**7**): 077304. DOI: 10.1088/1674-1056/ac560d

Light-modulated electron retroreflection and Klein tunneling in a graphene-based n-p-n junction

Xingfei Zhou(周兴飞), Ziying Wu(吴子瀛), Yuchen Bai(白宇晨), Qicheng Wang(王起程), Zhentao Zhu(朱震涛), Wei Yan(闫巍), and Yafang Xu(许亚芳)
Chin. Phys. B, 2022, 31 (**4**): 047301. DOI: 10.1088/1674-1056/ac2b94

Spin—orbit stable dirac nodal line in monolayer B_6O

Wen-Rong Liu(刘文荣), Liang Zhang(张亮), Xiao-Jing Dong(董晓晶), Wei-Xiao Ji(纪维霄), Pei-Ji Wang(王培吉), and Chang-Wen Zhang(张昌文)
Chin. Phys. B, 2022, 31 (**3**): 037305. DOI: 10.1088/1674-1056/ac4cba

Integer quantum Hall effect in Kekulé-patterned graphene

Yawar Mohammadi and Samira Bahrami
Chin. Phys. B, 2022, 31 (**1**): 017305. DOI: 10.1088/1674-1056/ac1b82

Electronic structure of molecular beam epitaxy grown 1T'-$MoTe_2$ film and strain effect

Xue Zhou(周雪), Zeyu Jiang(姜泽禹), Kenan Zhang(张柯楠), Wei Yao(姚维), Mingzhe Yan(颜明哲), Hongyun Zhang(张红云), Wenhui Duan(段文晖), Shuyun Zhou(周树云)
Chin. Phys. B, 2019, 28 (**10**): 107307. DOI: 10.1088/1674-1056/ab43ba

---

Valley-dependent transport in strain engineering graphene heterojunctions

Fei Wan(万飞)[1], X R Wang(王新茹)[1], L H Liao(廖烈鸿)[1], J Y Zhang(张嘉颜)[1], M N Chen(陈梦南)[1], G H Zhou(周光辉)[2], Z B Siu(萧卓彬)[3], Mansoor B. A. Jalil[3], and Yuan Li(李源)[1,†]

[1] *Department of Physics, Hangzhou Dianzi University, Hangzhou* 310018, *China*

[2] *Department of Physics and Key Laboratory for Low-Dimensional Quantum Structures and Manipulation (Ministry of Education), Hunan Normal University, Changsha* 410081, *China*

[3] *Computational Nanoelectronics and Nano-device Laboratory, Electrical and Computer Engineering Department, National University of Singapore, Singapore* 117576, *Singapore*

(Received 27 October 2021; revised manuscript received 28 January 2022; accepted manuscript online 17 February 2022)

We study the effect of strain on band structure and valley-dependent transport properties of graphene heterojunctions. It is found that valley-dependent separation of electrons can be achieved by utilizing strain and on-site energies. In the presence of strain, the values of transmission can be effectively adjusted by changing the strengths of the strain, while the transport angle basically keeps unchanged. When an extra on-site energy is simultaneously applied to the central scattering region, not only are the electrons of valleys K and K' separated into two distinct transmission lobes in opposite transverse directions, but the transport angles of two valleys can be significantly changed. Therefore, one can realize an effective modulation of valley-dependent transport by changing the strength and stretch angle of the strain and on-site energies, which can be exploited for graphene-based valleytronics devices.

Keywords: strain engineering, valley-dependent separation, graphene, on-site energy

PACS: 73.63.–b **DOI:** 10.1088/1674-1056/ac5613

1. Introduction

So far, extensive attention[1,2] has been given to graphene systems owing to the unique band structures and properties of graphene since it has been experimentally fabricated.[3,4] Pristine graphene is a zero-gap semiconductor and has a linear dispersion relationship near the Dirac points,[2,5] which cause electrons to behave as relativistic Dirac particles. It has also been experimentally verified that graphene has a remarkably high electron mobility at room temperature, which makes graphene an excellent semiconductor. Because of its exceptional electrical and thermal transport properties, graphene is an important two-dimensional material for exploration of physical phenomena in condensed matter,[2] and is expected to be very useful in the next-generation electronic devices.

Valley filtering effect is first reported in graphene nanoribbons,[6,7] which has been widely studied in various low-dimensional materials. Based on the semiclassical transport formulas, the valley-contrasting Berry phase effect has been taken into account in graphene nanoribbons.[8] There are also some beyond-graphene candidate materials for valleytronics applications, such as silicene,[9,10] black phosphorus,[11] and Weyl semimetals.[12,13] The interplay of spin and valley in transition-metal dichalcogenides (TMDs) can induce a valley-dependent spin-Hall effect[14] and large valley polarization.[15]

It is expected to modulate the valley-dependent transport by utilizing mechanical deformation in graphene systems.[16,17] The band structure does not change substantially for realistic strains of up to 15%.[18,19] The effect of long-range strain on electronic properties is a unique feature of graphene.[20,21] At low energies, the effects of strains can be modeled as a gauge field that acts as additional pseudo-magnetic field in the momentum operators.[22] The most obvious evidence for the unusual effects of strain on the electronic states comes from scanning tunneling microscope measurements of the electronic local density of states of graphene grown on platinum.[23] An average compression of 10% creates effective fields of the same order of magnitude as the pseudo-magnetic fields observed in experiments.[24]

Although these previous works have reported many interesting results on the properties of graphene systems under strain, the effect of strain on the valley-dependent transport and separation in graphene systems has not been extensively discussed. In this study, we adopt the tight-binding mode-matching method and propose an efficient way to separate the Dirac fermions in different valleys by utilizing strain and the on-site energy in graphene systems. Our results show that the electrons can be dispersed by strain and the on-site energy in a valley-dependent manner. The combination of strain and on-site energy can be used to realize the effective modulation of valley-dependent transport without the need for ferromagnetic materials or magnetic fields. This phenomenon provides an al-

[†]Corresponding author. E-mail: liyuan@hdu.edu.cn

© 2022 Chinese Physical Society and IOP Publishing Ltd

ternative route to effectively modulate the valley polarizations of graphene devices.

The paper is organized as follows: In Section 2, we consider a graphene heterojunction under the influence of strain and an on-site potential applied to the central scattering region. We then calculate the strain-modulated hopping parameters based on the Slater–Koster framework. In Section 3, we analyze the dispersion relations and employ the mode-matching method to investigate the valley-dependent angular transmission. The combined effects of strain and on-site energies on the valley separation are analyzed and discussed. Finally, a summary is given in Section 4.

2. Model and analysis of strain

We consider the dynamics of electrons hopping in the honeycomb lattice governed by the nearest-neighbor tight-binding Hamiltonian[25,26]

$$H = \sum_i \Omega c_i^\dagger c_i - \sum_{\langle i,j\rangle} t(\boldsymbol{\delta}_{ij}) c_i^\dagger c_j, \tag{1}$$

where c_i ($c_i^\dagger$) is the electron annihilation (creation) operator on the site i, the summation $\sum_{\langle i,j\rangle}$ is only over the nearest-neighboring sites, and $\boldsymbol{\delta}_{ij}$ is the vector linking the nearest-neighboring sites i and j. $\boldsymbol{\delta}_{ij}$ takes the values of $\pm\boldsymbol{\delta}_1$, $\pm\boldsymbol{\delta}_2$, or $\pm\boldsymbol{\delta}_3$ where $\boldsymbol{\delta}_{1,2,3}$ are shown in Fig. 1.

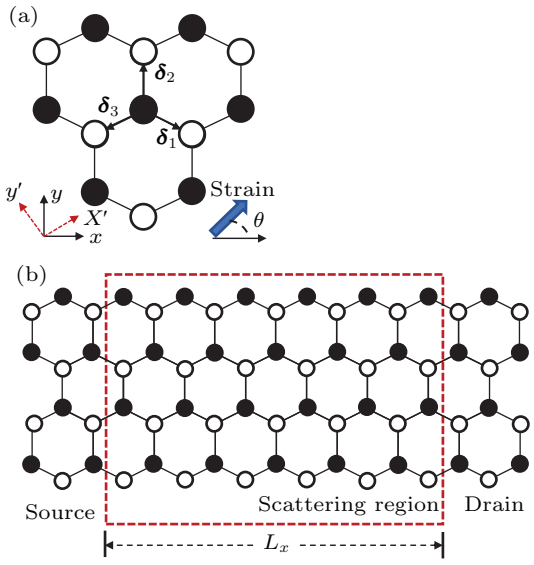


Fig. 1. (a) Honeycomb lattice geometry. The vectors $\boldsymbol{\delta}_1$, $\boldsymbol{\delta}_2$, $\boldsymbol{\delta}_3$ connect the A sites (white) to their B-site (black) neighbors. (b) Schematic of the graphene heterojunction with an applied uniaxial strain in the central scattering region. The zigzag direction of the honeycomb lattice (x–y plane) is parallel to the x axis, and the tension is applied at an angle θ relative to the x axis.

The first term in Eq. (1) is on-site potential energy with Ω being the magnitude of on-site energy. In practice, the on-site energy can be realized and tuned by applying top or bottom gates on the central graphene sheet. The second term is the nearest-neighbor hopping with the hopping energy $t(\boldsymbol{\delta}_{ij})$, where the dependence of t on $\boldsymbol{\delta}_{ij}$, the vector between two sites connected by t, is explicitly stated to reflect the fact that the applied strain breaks the isotropy of the honeycomb lattice and that of the coupling strengths between a given lattice site and its three neighbors. In the central scattering region, the graphene sheet is uniformly stretched (or compressed) along the angle θ relative to the x axis. Noticeably, we assume that there exists no strain outside the central scattering region.

In the considered Cartesian coordinates, the tension $\boldsymbol{T}$ can be written as $\boldsymbol{T} = T(\cos\theta\hat{e}_x + \sin\theta\hat{e}_y)$. It is convenient to introduce the principal coordinates $Ox'y'$, in which the tension is written as $\boldsymbol{T} = T\hat{e}_{x'}$. The strain ε'_{ij} is related to the components of the compliance tensor through the generalized Hooke's law[18] by $\varepsilon'_{ij} = TS_{ijxx}$, where the indices $i, j = x, y$. For the honeycomb lattice, only the five compliance tensor components S_{xxxx}, S_{xxyy}, S_{xxzz}, S_{zzzz}, S_{yzyz} are independent.[27] Thus, Poisson's transverse ratio is defined as $\nu = -S_{xxyy}/S_{xxxx}$. For simplicity, we choose Possion's ratio to be $\nu = 0.165$[18] in our numerical calculations.

It should be mentioned that when stress is mechanically induced in graphene by stretching the substrate, the relevant parameter is in fact the tensile strain rather than the tension T. For this reason, we treat ε as the tunable parameter. Because the lattice is oriented with respect to the Oxy axes, the stress tensor needs to be rotated to extract information about the bond deformations. The strain tensor in the lattice coordinate system reads

$$\xi = \varepsilon \begin{pmatrix} \cos^2\theta - \nu\sin^2\theta & (1+\nu)\cos\theta\sin\theta \\ (1+\nu)\cos\theta\sin\theta & \sin^2\theta - \nu\cos^2\theta \end{pmatrix}. \tag{2}$$

When the strain is applied to the graphene system, the lattice deformation will result in changes to the vectors $\boldsymbol{\delta}_\ell$ ($\ell = 1,2,3$). The strain-dependent vectors are given by $\boldsymbol{\delta}_\ell = (1+\xi)\cdot\boldsymbol{\delta}_\ell^0$, which thus modulate the hopping terms. Accordingly, we obtain the following deformed bond lengths:

$$|\boldsymbol{\delta}_1| = \left(1 + \frac{3}{4}\xi_{11} - \frac{\sqrt{3}}{2}\xi_{12} + \frac{1}{4}\xi_{22}\right)a_0, \tag{3}$$

$$|\boldsymbol{\delta}_2| = (1+\xi_{22})a_0, \tag{4}$$

$$|\boldsymbol{\delta}_3| = \left(1 + \frac{3}{4}\xi_{11} + \frac{\sqrt{3}}{2}\xi_{12} + \frac{1}{4}\xi_{22}\right)a_0, \tag{5}$$

where $\xi_{\kappa,\kappa'}$ ($\kappa = 1,2$) are the matrix components of the strain tensor ξ in Eq. (2), and $a_0 = 0.142$ nm is the distance between nearest-neighbor lattice sites in unstrained graphene.

The change in bond lengths leads to different hopping amplitudes between each site and its three nearest neighbors. In the Slater–Koster framework,[28] the hopping terms can be obtained from the dependence of the integral $V_{pp\pi}$ on the inter-orbital distance. A more convenient assumption is an exponential decay. Thus, we assume that, in graphene,[18]

$$t(\boldsymbol{\delta}_\ell) \simeq V_{pp\pi}(r_\ell) = t_0\, \mathrm{e}^{-3.37(r_l/a_0-1)}, \tag{6}$$

where $r_\ell = |\delta_\ell|$ is the bond length, and the hopping energy t_0 is 2.7 eV. We calculate the conductance of graphene using the Landauer formula[29]

$$G = \frac{e^2}{h}\sum_{m=-N}^{N} T_m, \quad T_m = \sum_{n=-N}^{N} |t_{n,m}|^2. \tag{7}$$

Here $t_{n,m} = \tilde{\psi}^{\dagger}_{R,n}(+)G_{S+1,0}[G^{(0)}_{0,0}]^{-1}\psi_{L,m}(+)$, with $\psi_{R/L,n}(+)$ being the nth right-going propagating mode of the right (left) lead and $\tilde{\psi}_{R/L,n}(+)$ its dual vector. The left lead is coupled to the system at site 0, and the right lead at site $S+1$. $G^{(0)}$ and G refer to Green's functions of the left lead and the full system, respectively, which can be obtained by using iterative Green's function approach.[30,31] After obtaining Green's functions, the valley-resolved transmission can be calculated. The K and K' valleys[6,32,33] can be distinguished by the wavevector k_x of the incident source mode $\psi_{L,m}(+)$. Here, $\psi_{L,m}(+)$ lies in the first valley K if its wave vector is in the range of $k_x a \in (0,\pi)$, and in the second valley K' if its wave vector lies within the range of $k_x a \in (\pi, 2\pi)$ where $a = \sqrt{3}a_0$.

Utilizing periodic boundary conditions along the transverse direction, an infinite graphene sheet can be modeled using a graphene nanoribbon with the zigzag chain number of $N_y = 2$.[34] There exists an extra hopping term between the sites at the transverse boundaries, which are wrapped around and so as to overlap with each other. Thus we can introduce a Bloch phase factor $e^{i3k_y a_0}$ to modify these hopping terms with k_y being the Bloch wave vector. The incident angle is defined as $\phi = \arcsin(k_y/k_F)$, where the Fermi wave vector k_F can be obtained from the relation $k_F = 2E_F/(3a_0 t)$.

3. Numerical results and discussion

We consider a heterojunction containing a strained central scattering region sandwiched between two unstrained leads, as shown in Fig. 1. The length of the strained graphene section along the longitudinal direction is denoted as L_x, where $L_x = [(W_x - 1)/2] \times \sqrt{3}a_0$ and W_x, the number of distinct rows of atoms along x direction of the sheet is fixed at $W_x = 1001$.

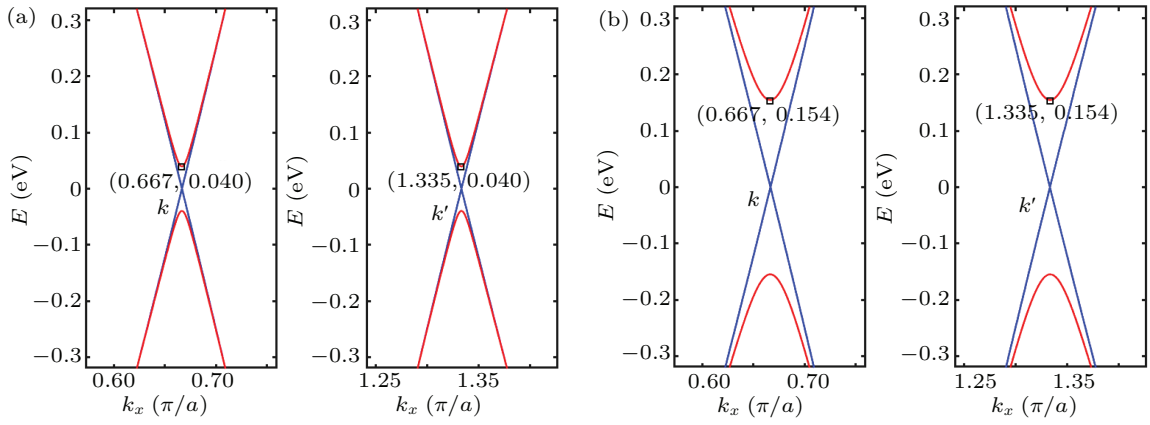


Fig. 2. Dispersion relations plotted as a function of the wave vector k_x for (a) $\varepsilon = 0.002$ and (b) $\varepsilon = 0.02$. The other parameters are $\nu = 0.165$, $\theta = 45°$, $\Omega = 0$ and $k_y = 0$. The red (blue) curve denotes the presence (absence) of the applied strain.

3.1. Influence of the strain on band structures

We investigate the dispersion relation of the infinite-size homogeneous graphene sheet under the influence of the strain ε. The dispersion relations at $k_y = 0$ are shown in Fig. 2. In the absence of strain, there is no band gap in energy bands [see blue curves] at K and K' valleys. When $\varepsilon = 0.002$, the energy difference between the bottom of conduction band and the top of valence band increases to about 80 meV [see red curves in Fig. 2(a)]. With the strength of strain increasing to $\varepsilon = 0.02$, the energy difference is significantly enlarged to about 308 meV.

It is natural to ask if the minima of the energy profiles for the two valleys still occur at $k_y = 0$ in the presence of strain. To clarify the effect of the strain on Dirac points, we plot equal-energy contours as a function of the wave vectors k_x and k_y at different strain strengths in Fig. 3. We can see that when $\varepsilon = 0$, the Dirac points of K and K' valleys are located at $(k_x, k_y) = (0.667, 0)$ and $(1.332, 0)$, respectively. When the strain increases from $\varepsilon = 0$ to 0.005 in Fig. 3(b), the Dirac point of K valley moves towards smaller value of k_x and negative value of k_y, while the Dirac point K' moves towards the opposite direction. Interestingly, in Figs. 3(b)–3(d), the Dirac points of K and K' valleys gradually deflect from the axis of $k_y = 0$ along negative direction as the strain increases from $\varepsilon = 0$ to 0.005, 0.015 and 0.03. It is obvious that the valley separation and transverse shifts of Dirac cones increase with the increasing strain. Because the dispersion relations in Fig. 2 depict only a cut of the Dirac cone at $k_y = 0$, the energy difference between the top of valence band and the bottom of conduction band does not refer to the real band gap.

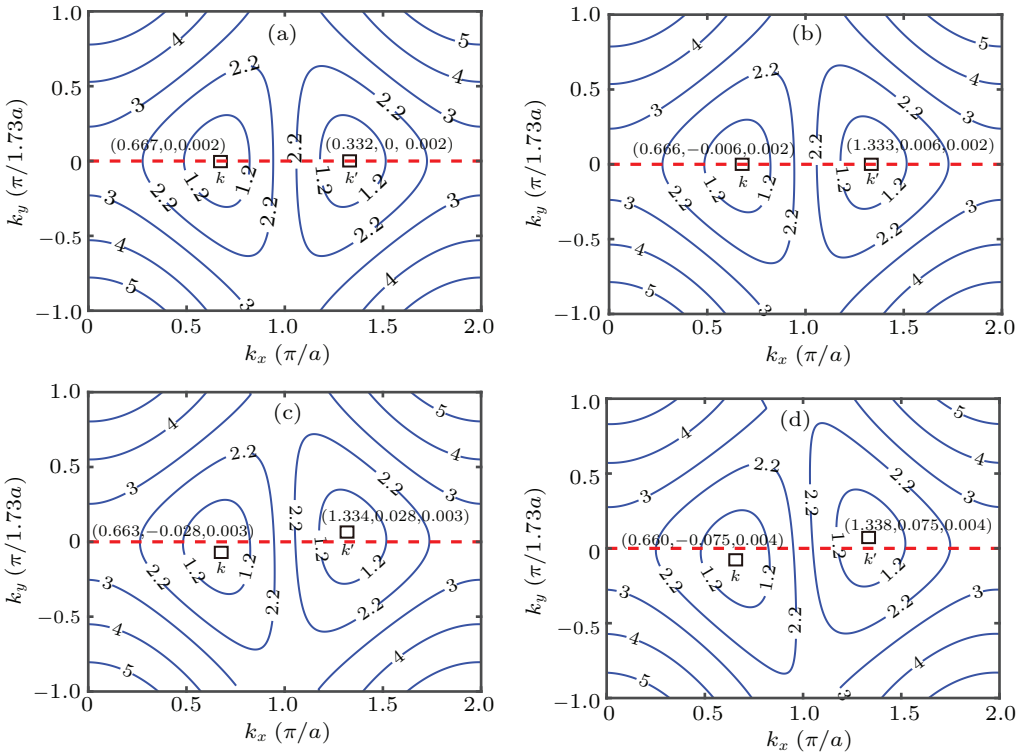


Fig. 3. Contour plot of the energies as a function of the wave vectors k_x and k_y for different strain strengths: (a) $\varepsilon = 0$, (b) $\varepsilon = 0.005$, (c) $\varepsilon = 0.015$, and (d) $\varepsilon = 0.03$. The solid lines are equal-energy contour lines corresponding to energy values of 1.2 eV, 2.2 eV, 3 eV, and 4 eV. The other parameters are $\Omega = 0$, $\nu = 0.165$, and $\theta = 45°$. The black squares denote the positions of Dirac points of K and K' valleys with the value of (k_x, k_y, E).

3.2. Effect of the strain on the valley-dependent transmission

Next we further study the effect of strain on the transport properties for the stretched angle $\theta = 30°$ in the absence of potential energy in the central scattering section. When $\varepsilon = 0$, as shown in Fig. 4(a), the transmissions of K and K' valleys are identical and equal to 1. In this case the graphene system is homogenous in the absence of any impurities and external disturbances, and the electrons are correspondingly completely transmitted without reflection. When ε is increased to 0.003, the transmission curve of K valley is deflected downwards, while that of K' valley is deflected upwards. Moreover, the maximum value of the transmission is significantly reduced to about 0.15 because of the strain. Because the graphene system is no longer a homogeneous system under the influence of the strain, which leads to the relative shift of two Dirac cones and the non-perfect transmission of electrons in two valleys. These results imply that the strain can be used to separate the Dirac fermions in the K and K' valleys, which is similar to the deflection behavior induced by magnetic fields.[35–37]

In Fig. 5, we plot the transmissions of valleys K and K' versus the incident angle ϕ for different stretching angles θ when $\Omega = 0$. It is obvious that the transmission curves of K (K') valley are deflected downwards (upwards) for positive incident angles from $\theta = 0°$ to 30°, as shown in Fig. 5. However, as the stretching angle increases, the value of the valley-dependent transmission decreases sharply, while the incident angle associated with large values of the transmission basically keeps unchanged. When the angle is changed to negative values of $\theta = 0°$ to $-30°$, the transmission profiles of K and K' valleys are pushed upwards and downwards, respectively. When the strain is applied along the zigzag ($\theta = 0°$) or armchair direction $\theta = 90°$ ($-90°$), the transmission profiles of two valleys are symmetrical with respective to the normal incident. The electrons in K and K' valleys therefore cannot be separated at these strain configurations. The results show that the valley-dependent transmission of electrons can be effectively tuned by changing the stretching angle in the absence of the on-site energy.

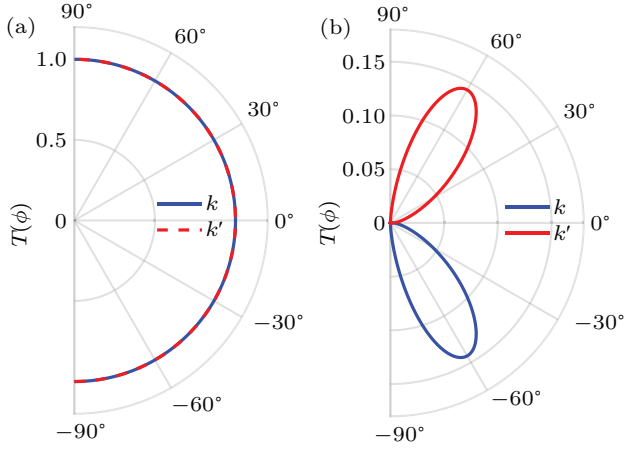


Fig. 4. Valley-dependent transmission plotted as a function of the incident angle ϕ for (a) $\varepsilon = 0$ and (b) $\varepsilon = 0.003$. The other parameters are $E_F = 15$ meV, $\theta = 30°$, $\Omega = 0$ and $L_x = 123$ nm.

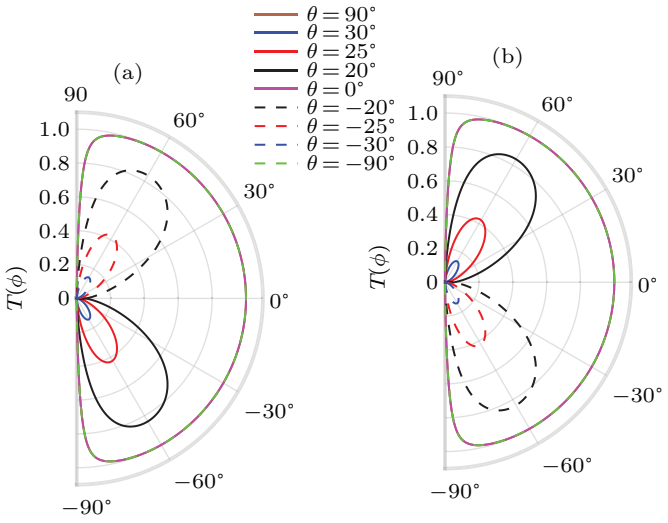


Fig. 5. The transmission of (a) K and (b) K' valleys plotted as a function of the incident angle ϕ for different stretching angles θ. The other parameters are $E_F = 15$ meV, $\varepsilon = 0.003$, $\Omega = 0$ and $L_x = 123$ nm.

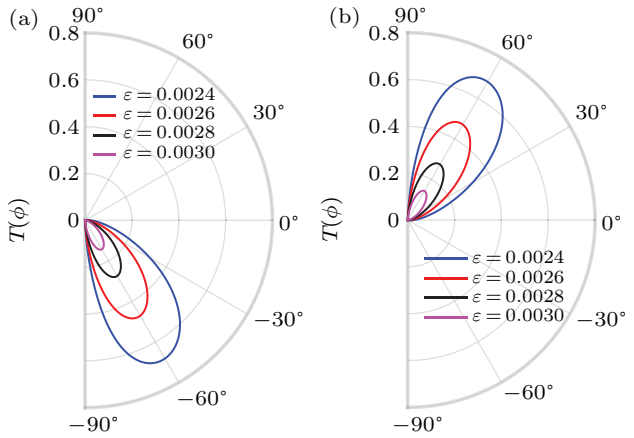


Fig. 6. (a) The K and (b) K' valley dependence of the transmission versus the incident angle ϕ for different strengths of the strain. The other parameters are $E_F = 15$ meV, $\theta = 30°$, $\Omega = 0$, and $L_x = 123$ nm.

To clarify the effect of the strain strength on the valley-dependent transport when $\Omega = 0$, we plot the transmission of K and K' valleys as a function of the incident angle ϕ for different values of the strain strengths in Fig. 6. We find that the transmission profile of K (K') valley is deflected downwards (upwards) by the strain. As the strain increases from $\varepsilon = 0.0024$ to $\varepsilon = 0.003$, the transmission magnitude of the electrons decreases gradually, but the symmetry axes of the transmission lobes are not deflected. The transmission curve of K valley remains within the angle interval $-75° < \phi < -25°$ [see Fig. 6(a)] and that of the K' valley remains within the angle interval $25° < \phi < 75°$ over the ranges of strain strengths [see Fig. 6(b)]. These results imply that when the on-site energy is zero, the transmission profile does not exhibit a deflection behavior, and the valley-dependent transmission of electrons decreases with the increasing strain strength.

Based on the above analysis, when $\Omega = 0$, strain can effectively cause the separation of the transmission profiles of the electrons in the two valleys, and the valley-dependent transport behavior can be effectively tuned by changing the strength of the strain. However, the symmetry axes of transmission profiles of two valleys remain unchanged when the strain angle or strength of the strain is varied.

3.3. Combined effect of the strain and on-site energy

In the above section, we can see that the strength of the strain can be used to effectively tune the valley-dependent transmission, but the change in the symmetry axis of the transmission profile is not obvious. We thus further study the combined effect of the strain and the on-site energy on the transport property. In Fig. 7(a), when $\Omega = 0$, the transmission curve of K (K') valley is deflected downwards (upwards), and the maximum value of the transmission is about 0.15. In Fig. 7(b), when the on-site energy increases to $\Omega = 25$ meV, the transmission lobe of K valley is centered around $\phi = -63°$, while the transmission lobe of K' valley is centered around $\phi = 63°$. Moreover, the addition of the on-site energy significantly increases the maximum value of the transmission to 1. The on-site potential energy results in the formation of an n–p–n type heterojunction, which in turn leads to the recovery of perfect Klein tunneling in the considered system. These results imply that the on-site energy can result in the concentration of the electron transport in K and K' valleys in one special direction and significantly increase the transmission amplitudes, which is similar to the deflection behavior induced by electric fields in silicene systems.[10]

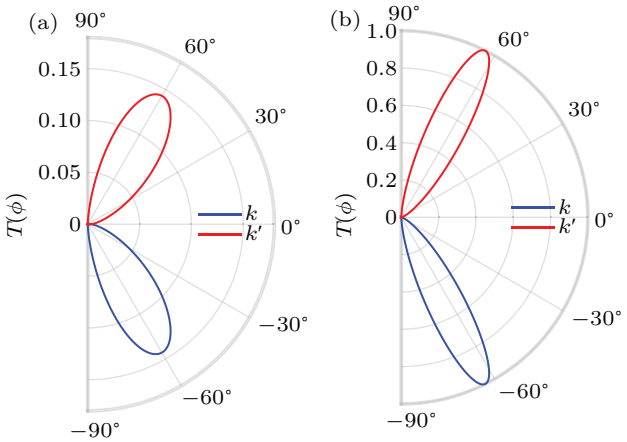


Fig. 7. Valley-dependent transmission plotted as a function of the incident angle ϕ for (a) $\Omega = 0$ and (b) $\Omega = 25$ meV. The other parameters are $E_F = 15$ meV, $\theta = 30°$, $\varepsilon = 0.003$, and $L_x = 123$ nm.

To illustrate the effect of the on-site energy on the valley-dependent transport properties, Fig. 8 shows the contour plots of the transmission of K and K' valleys as a function of the on-site energy Ω and the transverse wave vector k_y for different strain strengths. For each subgraph in Fig. 8, the left and right panels are respectively associated with K and K' valleys. In this numerical calculation, $\theta = 30°$ and $E_F = 15$ meV. In

Fig. 8(a), when $\varepsilon = 0$, electrons in both valleys undergo perfect transmission through the graphene heterojunction at normal incidence irrespective of the values of Ω, which is a characteristic of Klein tunneling. It is obvious that the transmission contour plot is symmetrical about $\phi = 0$. Interestingly, there exists a region at $10 < \Omega < 30$ meV in which the incident angle range with large transmission is contracted. As the strain increases from $\varepsilon = 0.001$ to $\varepsilon = 0.003$, the regions with large transmission values for the K valley gradually becomes tilted downwards, while that of K' valley moves upwards. This tilted trend is particularly obvious in the contraction region within the interval of $10 < \Omega < 30$ meV, which shows a significant effect of the strain and on-site energy.

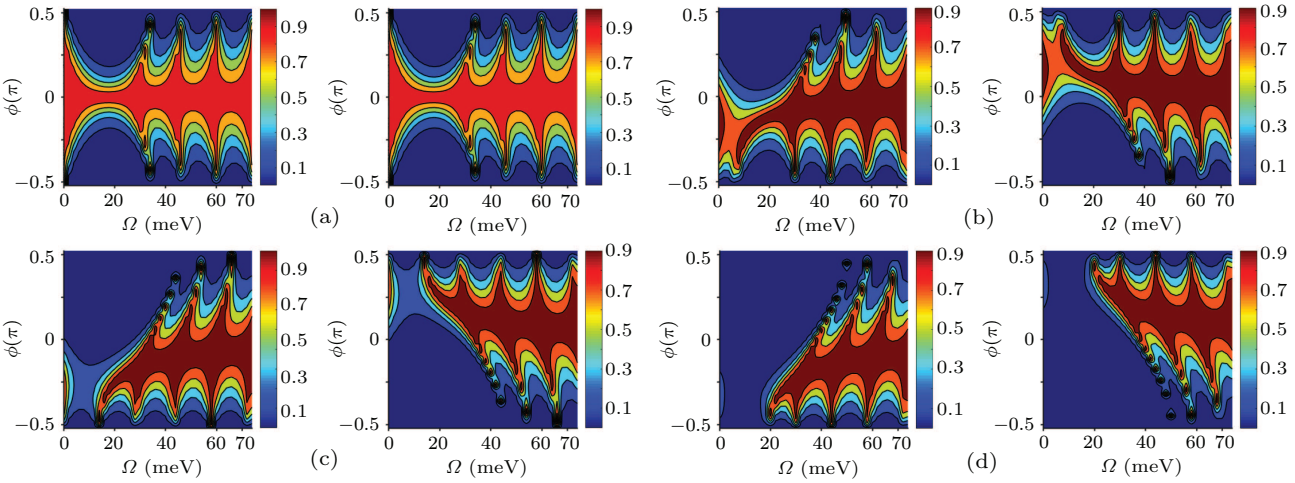


Fig. 8. Contour plots of the valley-dependent transmission of the graphene heterojunction as a function of the on-site energy Ω and the incident angle ϕ for different strain strengths: (a) $\varepsilon = 0$, (b) $\varepsilon = 0.001$, (c) $\varepsilon = 0.002$, (d) $\varepsilon = 0.003$. The other parameters are $v = 0.165$, $\theta = 30°$, and $L_x = 123$ nm. For each panel, the left and right subgraphs are associated with K and K' valleys, respectively.

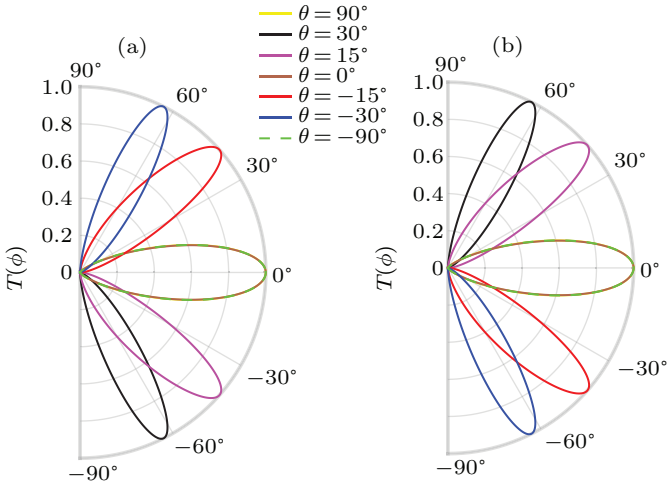


Fig. 9. The transmission of (a) K and (b) K' valleys plotted as a function of the incident angle ϕ for different stretching angles θ. The other parameters are $E_F = 15$ meV, $\varepsilon = 0.003$, $\Omega = 25$ meV, and $L_x = 123$ nm.

Correspondingly, we further study the effect of the stretching angle θ on the valley-dependent transport at $\Omega = 25$ meV, as shown in Fig. 9. We find that the transmission curves of K (K') valley are deflected downwards (upwards) from $\theta = 0°$ to $30°$. However, when the stretching angle is changed to negative values, from $\theta = 0°$ to $-30°$, the transmission profiles of K and K' valleys are respectively pushed upwards and downwards, respectively. When the stretching angle is increased, the transmission curves shift to larger incident angles. When the strain is applied along the zigzag or armchair direction, i.e., at $\theta = 0°$ or $90°$ ($-90°$), the transmission profiles of two valleys are symmetrical about $\phi = 0°$, and there is no deflection behavior, which is a distinct anisotropy behavior for the strain modulation of the valley current. Thus, the electrons of K and K' valleys are not separated at these strain configurations. It can be seen that the valley polarization can be effectively modulated by changing the stretching angle of the strain.

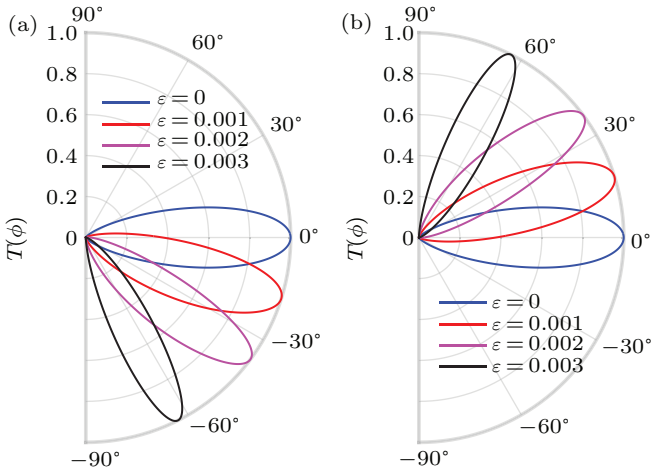


Fig. 10. The transmission of (a) K and (b) K' valleys is plotted as a function of the incident angle ϕ for different strengths of the strain. The other parameters are $E_F = 15$meV, $\theta = 30°$, $\Omega = 25$ meV, and $L_x = 123$ nm.

Similar results can be seen in Fig. 10. We plot the transmission of K and K' valleys as a function of the incident angle ϕ for different strengths of the strain when $\Omega = 25$ meV. We find that the transmission profile of K valley is deflected down-

wards as the strain is increased from 0.001 to 0.003, which differs from the results in Fig. 6 in which the incidence angle for the peak transmission is independent of the strain magnitude. For example, when $\varepsilon = 0.002$, the incident angles at which electrons will be transmitted is pushed towards the angular region of $\phi < -30^\circ$ [see Fig. 10(a)]. This implies that the K-valley electrons will be scattered back into the left region if the incident angle is larger than a certain critical angle. The transmission profile of K' valley is correspondingly deflected upwards under the influence of the strain. The K'-valley electrons will be deflected back into the incident region when the incident angle is smaller than a certain angle.

Based on the above analysis, when the on-site energy is not zero, strain can be used to effectively separate electrons from different valleys, and the incident angles with high values of the transmission effectively adjusted by changing the angle and strength of the strain. This finding is of great significance for graphene-based valleytronics devices.

4. Conclusions

In summary, we have studied the effects of the strain and on-site energy on the dispersion relation and transport properties of graphene heterojunctions. It is found that the electrons can be dispersed in a valley-dependent manner by the uniaxial strain. When the on-site energy is zero and only strain acts on the graphene system, the transmission profiles are deflected to two opposite transverse directions, resulting in the separation of K and K' valleys. When the strengths of the strain are changed, the magnitude of the transmission is significantly affected by the strain, but the transport angles associated with large values of the transmission are basically keep unchanged. When an additional on-site energy is applied to the scattering region, not only are the electrons in the K and K' valleys separated into two branches, but the transport angle of the electrons are also changed significantly as the angle and strength of the strain increases. Therefore, by combining the strain and on-site energy, an effective modulation of the valley-dependent transport can be achieved by changing the strength and direction of the strain. Our results may be helpful for exploring the transport mechanism of strain-modulated graphene systems and the design of novel types of graphene-based valleytronics devices.

Acknowledgement

Project supported by National Natural Science Foundation of China (Grant No. 11574067).

References

[1] Bolotin K I, Sikes K J, Jiang Z, Fudenberg G, Hone J, Kim P and Stormer H L 2008 *Solid State Commun.* **146** 351
[2] Neto A H C, Guinea F, Peres N M R, Novoselov K S and Geim A K 2009 *Rev. Mod. Phys.* **81** 109
[3] Novoselov K S, Geim A K, Morozov S V, Jiang D, Zhang Y, Dubonos S V, Grigorieva I V and Firsov A A 2004 *Science* **306** 666
[4] Geim A K and Novoselov K S 2007 *Phys. Today* **60** 35
[5] Wallace P R 1947 *Phys. Rev.* **71** 622
[6] Rycerz A, Tworzydlo J and Beenakker C W J 2007 *Nat. Phys.* **3** 172
[7] Castro Neto A H, Guinea F, Peres N M R, Novoselov K S and Geim A K 2009 *Rev. Mod. Phys.* **81** 109
[8] Xiao D, Yao W and Niu Q 2007 *Phys. Rev. Lett.* **99** 236809
[9] Ezawa M 2012 *Phys. Rev. Lett.* **109** 055502
[10] Li Y, Zhu H B, Wang G Q, Peng Y Z, Xu J R, Qian Z H, Bai R, Zhou G H, Yesilyurt C, Siu Z B and Jalil M B A 2018 *Phys. Rev. B* **97** 085427
[11] Ang Y S, Yang S A, Zhang C, Ma Z S and Ang L K 2017 *Phys. Rev. B* **96** 245410
[12] Parameswaran S A, Grover T, Abanin D A, Pesin D A and Vishwanath A 2014 *Phys. Rev. X* **4** 031035
[13] Yesilyurt C, Siu Z B, Tan S G, Liang G, Yang S A and Jalil M B A 2019 *Sci. Rep.* **9** 4480
[14] Shan W Y, Lu H Z and Xiao D 2013 *Phys. Rev. B* **88** 125301
[15] Zhang Q Y, Yang A S Y, Mi W B, Cheng Y C and Schwingenschlogl U 2016 *Adv. Mater* **28** 959
[16] Seon-Myeong C, Seung-Hoon J and Young-Woo S 2010 *Phys. Rev. B* **81** 081407
[17] Wu B L, Wei Q, Zhang Z Q and Jiang H 2021 *Chin. Phys. B* **30** 030504
[18] Pereira V M, Castro Neto A H and Peres N M R 2009 *Phys. Rev. B* **80** 045401
[19] Lee C, Wei X, Kysar J W and Hone J 2008 *Science* **321** 385
[20] Suzuura H and Ando T 2002 *Phys. Rev. B* **65** 235412
[21] Manes J L 2007 *Phys. Rev. B* **76** 045430
[22] Vozmediano M A H, Katsnelson M I and Guinea F 2010 *Phys. Rep.* **496** 109
[23] Levy N, Burke S A, Meaker K L, anlasigui M, Zettl A, Guinea F, Castro Neto A H and Crommie M F 2010 *Science* **329** 544
[24] Abedpour N, Asgari R and Guinea F 2011 *Phys. Rev. B* **84** 115437
[25] Song J T, Liu H W, Jiang H, Sun Q F and Xie X C 2012 *Phys. Rev. B* **86** 085437
[26] Bahamon D A, Pereira A L C and Schulz P A 2011 *Phys. Rev. B* **83** 155436
[27] Blakslee O L, Proctor D G, Seldin E J, Spence G B and Weng T 1970 *J. Appl. Phys.* **41** 3373
[28] Slater J C and Koster G F 1954 *Phys. Rev.* **94** 1498
[29] Ando T 1991 *Phys. Rev. B* **44** 8017
[30] Datta S 1995 *Electronic Transport in Mesoscopic Systems* (Cambridge: Cambridge University Press)
[31] Khomyakov P A, Brocks G, Karpan V, Zwierzycki M and Kelly P J 2005 *Phys. Rev. B* **72** 035450
[32] Cheng S, Liu H, Jiang H, Sun Q F and Xie X C 2018 *Phys. Rev. Lett.* **121** 156801
[33] Qin M S, Zhu P F, Ye X G, Xu W Z, Song Z H, Liang J, Liu K H and Liao Z M 2021 *Chin. Phys. Lett.* **38** 017301
[34] Li Y, Wan Q, Peng Y Z, Wang G Q, Qian Z H, Zhou G H and Jalil M B A 2015 *Sci. Rep.* **5** 18458
[35] De Martino A, Dell'Anna L and Egger R 2007 *Phys. Rev. Lett.* **98** 066802
[36] Masir M R, Vasilopoulos P and Peeters F M 2008 *Appl. Phys. Lett.* **93** 242103
[37] Li Y, Jalil M B A and Zhou G H 2014 *Appl. Phys. Lett.* **105** 193108